IEEE Access
Multidisciplinary | Rapid Review | Open Access Journal

Received July 22, 2019, accepted August 5, 2019, date of publication August 13, 2019, date of current version August 28, 2019.

Digital Object Identifier 10.1109/ACCESS.2019.2935101

A New Traction Motor System With Integrated-Gear: A Solution for Off-Road Machinery

JUHO MONTONEN[1], JANNE NERG[1], (Senior Member, IEEE), MEHMET GULEC[1,2], (Student Member, IEEE), AND JUHA PYRHÖNEN[1], (Senior Member, IEEE)

[1]Department of Electrical Engineering, Lappeenranta University of Technology, 53850 Lappeenranta, Finland
[2]Department of Electrical Engineering, Kocaeli University, 41380 Kocaeli, Turkey

Corresponding author: Juho Montonen (juho.montonen@lut.fi)

ABSTRACT Off-road traction applications require extremely high torque, especially, at low speeds. Such a high torque can be reached by gearing up the torque of an electrical machine. A tooth-coil permanent magnet synchronous machine with an integrated planetary gear is proposed as a solution for heavy off- and on-road traction applications. The key benefits of tooth-coil permanent-magnet synchronous machine (PMSM) in the proposed drive system and its integration with a planetary gearbox are explained in detail. A multi-objective optimization is performed to determine the slot/pole combination of the PMSM and the design process of the proposed drive system is entirely clarified. The proposed tooth-coil PMSM is investigated by electromagnetic and structural finite element analysis to obtain the final design and highlight the machine performance. A prototype is built to validate the proposed system. The results show that the traction drive system works well in laboratory and offers means to serve as a traction system in heavy off- and on-road applications.

INDEX TERMS Permanent magnet machines, traction motors, torque, planetary gear.

I. INTRODUCTION

Both high-torque, low-speed and high-speed, low-torque operations are needed in heavy off-road machinery. A typical example is an agricultural tractor that requires very high torque for ploughing on fields and relatively high speeds in on-road driving. Generally, torque ratio ($T_{\text{min speed}}/T_{\text{max speed}}$) may vary in the range of 20:1 or even 30:1. This can be easily judged by seeing the gear ratios of traditional off-road machines. An internal combustion engine (ICE) -based mechanical traction system delivers the engine power to the wheels via a mechanical drive train, which in principle provides a constant power drive for the whole speed range. The ICE-based mechanical or hydraulic traction has been used for decades in off-road applications. However, demand for better controllability and higher traction efficiency promote electrical traction applications [1]–[4].

A principal torque comparison of an ICE-based mechanical traction with a six-step gear and a typical electrical machine is given in Fig. 1. A comparison of the torque producing capability between the ICE traction and the electric machine in constant-flux and in field-weakening range is provided in the figure as a per-unit presentation with one (1) as the design speed and torque. The competition between the ICE traction and the electric machine traction appears mostly at low speeds. In a heavy vehicle, it is a hard task for an electric machine to achieve competitively high torques at low speeds if an electric drive train replaces a mechanical or hydraulic one. However, contrary to ICE the electric machine has a high overload ability, if only the motor winding and insulation temperatures remain at acceptable levels. Actually, an electric motor may compete with the ICE-gearbox curve in on-road applications, as the overloading at low speeds is intermittent. However, if an off- and on-road application is considered, the torque and speed ranges Fig. 1) are far from adequate. The per-unit torque for an off- and on-road application at its maximum speed is e.g. in the range of 0.33.

The associate editor coordinating the review of this article and approving it for publication was Bora Onat.

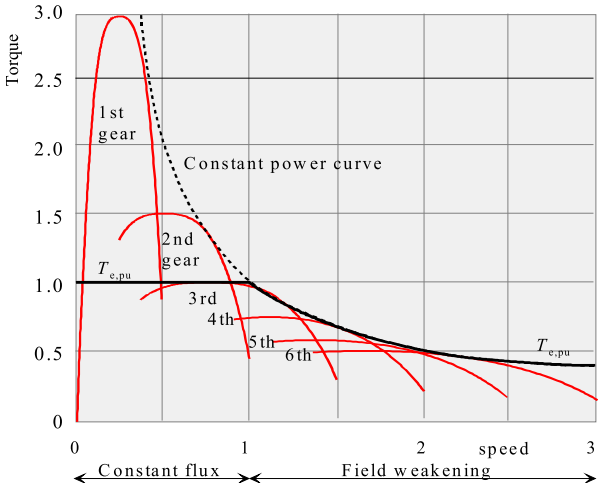

FIGURE 1. Comparison of the torque output of an ICE equipped with a six-step-gear and the torque of a typical electric traction on-road machine with the rated torque $T_e = 1$ and rated speed $\Omega = 1$. The ICE gear-output torque envelope curve follows constant power. The maximum torque for both traction systems is $T_{max} = 3$ and the maximum speed is $\Omega_{max} = 3$ at which the output torque is $T_{max\,\Omega} = 1/3$. This makes a total torque ratio $T_{start}/T_{max\,\Omega} = 3/(0.33) = 9/1$. This is, however, not enough for an off-road machine requiring e.g. $T_{start}/T_{max\,\Omega} = 36/1$.

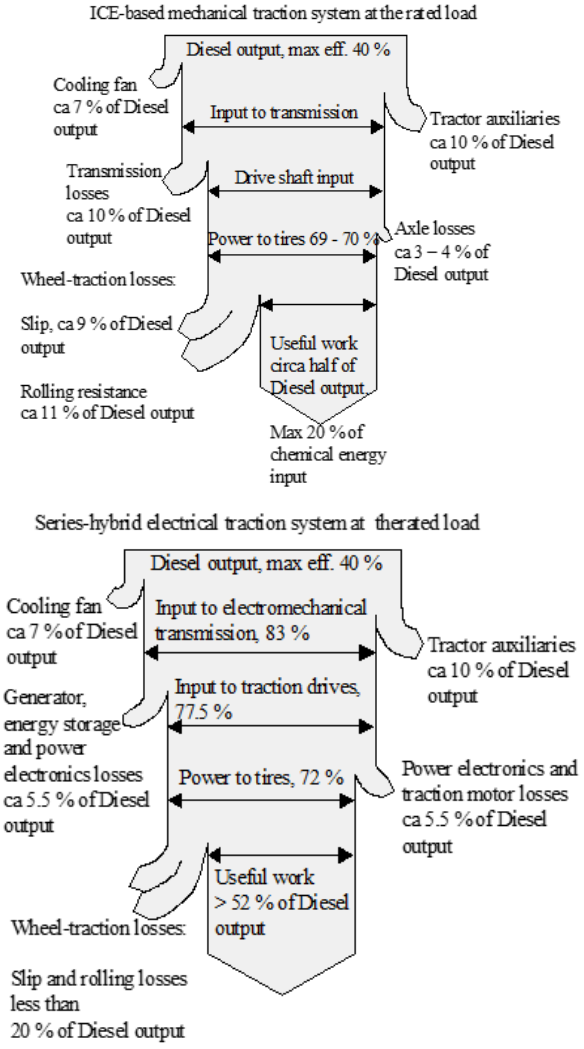

FIGURE 2. Sankey diagram of a typical agricultural tractor and a similar electromechanical drive train operating at its full power on a field. The numerical values found in the Fig. can be generally found in the literature concerning off-road machines [13].

If an electric motor has a per-unit starting torque of 3, it must be multiplied by e.g. a factor of 4 to achieve a high-enough general torque ratio (12:0.33 = 36:1). Therefore, a unique design solution is essential to overcome the above task and this is the motivation of this paper.

The authors have found a solution to integrate a two-step planetary gearbox inside a thin rim tooth-coil permanent magnet synchronous machine (TCPMSM) which has its own advantages widely reported in the literature [5]–[8]. Also different kinds of magnetic gear solution are studied in [9]–[11] but a mechanical gear was selected in this analysis because of its low price, large torque tolerance and robustness. It is often stated that a mechanical gear has lots of losses but different authors have shown with several measurements in [12] that the selected two step planetary gear has low losses.

The energy efficiency of an ICE-based mechanical four-wheel traction suffers from the fixed slip arranged between the front and rear wheels. Typically, the front wheels have ca 5 % higher peripheral speed than the rear wheels to make taking corners possible. This constant slip is seen in the high traction losses of the system. Figure 2 illustrates a typical Sankey diagram in an ICE-based mechanical traction system and a series hybrid electric drive-train system.

Figure 2 illustrates how the diesel output power is shared in a present-day traction system and in a series-hybrid traction system. The transmission, axle and traction losses consume a third of the diesel output. In case of a series-hybrid traction system operating at its full power there are conversion losses in the generator, electric energy storage, converters and traction motors. The typical rated point efficiency of a generator should be in the range of 97 %. The present-day IGBT converter efficiency is in the range of 98 %, electric energy storage efficiency is in practice very high as only part of electricity is travelling through it and an in-wheel 50 kW traction motor rated point efficiency should be in the range of 95 %. Therefore, the electric drive train losses should be about 9 % of the diesel output if the cooling and auxiliary systems' consumption is kept the same.

As better controllability of the wheel torque enables lower wheel-traction losses, the total electric traction can be slightly more efficient than the present-day system. This brings another motivation to develop the key drive-train component the integrated gear permanent magnet traction motor for off- and on-road machines. Naturally, an electric drive train enables very different construction for a future off-road machine as the boundary conditions set by the mechanical drive train are removed. The electric drive train also enables optimal usage of the power plant bringing extra efficiency benefits for the system.

In this paper, we concentrate on a feasible solution for an off-road traction motor system. The torque and power demand of a large agricultural tractor or similar can be solved by integrating a TCPMSM and a gearbox. The main contribution of this paper is to propose a practical and sustainable alternative to conventional ICE-based mechanical traction by a traction motor with an integrated gearbox enabling building a hybrid drive train for an off- and on-road machine.

The proposed traction motor system has two key components, which are the electric machine and the gearbox. The third important component is an electromagnetic gear shifting system enabling fast gear ratio change controlled by the frequency converter. A commercially available planetary gear is used and therefore its design is not reported here in details.

The selection of a tooth-coil PMSM topology and its design procedure, however, are explained in details. The theory of the proposed application is presented in Section II. Design of a TCPMSM is given in the next section. The finite element analysis (FEA) of the proposed TCPMSM is investigated in Section IV and experimental verification of the proposed drive system is described in the last section.

II. PROPOSED TRACTION MOTOR SYSTEM

In principle, there are some theoretical alternatives to reach such a torque-speed range (36:1) as presented in the introduction section. The first one is a high-speed electric machine with high enough speed and power resources and a high-gear-ratio reduction gear to adjust the wheel speed. The second one is a very large electric machine that can produce the starting torque needed and can also go deep in the field weakening. The torque ratio 20:1 − 30:1 is challenging from both the high-speed drive and the direct drive point of view; either the motor should become too large or its speed range should be difficult for the reduction gear. In case of a high-speed motor, the gear should in turn, become bulky. The third one is a normal speed range electric motor with an integrated gearbox. The last alternative is studied here.

Permanent magnet motor technology is applied and the following analysis is done fully in per-unit values. A permanent magnet synchronous machine can be designed to operate in a wide speed range by selecting its per-unit characteristic current, $i_{\mathrm{x,pu}}$, depending on the permanent magnet flux linkage, $\psi_{\mathrm{PM,pu}}$, and synchronous inductance, $L_{\mathrm{s,pu}}$, close to unity. The characteristic current is defined as

$$i_{\mathrm{x,pu}} = \frac{\psi_{\mathrm{PM,pu}}}{L_{\mathrm{s,pu}}}. \tag{1}$$

If $i_{\mathrm{x,pu}} = 1$ the theoretical speed range of the machine is infinite as its stator flux linkage can be driven to zero with the rated current without overheating the machine. In principle, such a motor should be capable of fulfilling the targets of the first and the second case. Despite this kind of selection, the practical solution might have difficulties in providing a practical torque-speed range needed. If the synchronous inductance $L_{\mathrm{s,pu}}$ of a PMSM is selected high, the motor may be overloaded only at the lowest speeds and its torque capabilities already at moderate speeds are limited based on the load angle δ equation and the voltage limit defined as

$$P_{\mathrm{pu}} = \frac{e_{\mathrm{PM,pu}} u_{\mathrm{s,pu}}}{\omega_{\mathrm{s,pu}} L_{\mathrm{s,pu}}} \sin\delta \tag{2}$$

where $e_{\mathrm{PM,pu}}$ is the permanent magnet induced voltage, $u_{\mathrm{s,pu}}$, the supply voltage ($u_{\mathrm{s,pu\,max}} = 1$) and $\omega_{\mathrm{s,pu}}$ the angular velocity in per-unit values. This simplified equation is used in the analysis since the machine presented in this paper has only 10 % of its torque coming from the rotor asymmetry coming from the fact that the d- and q-axis inductances do not have a significant difference. With high $L_{\mathrm{s,pu}}$, the field weakening starts well before the rated voltage no-load speed if $\psi_{\mathrm{PM,pu}} = 1$. If a typical distributed winding machine is assumed with e.g. $\psi_{\mathrm{PM,pu}} = 1$, $L_{\mathrm{md,pu}} = 0.7$ and $L_{\mathrm{s,pu}} = 0.85$ and we neglect saturation, the torque range can probably be increased up to 9:1 as in Fig. 1 but this is still far from the desired minimum torque range (20:1 . . . 40:1) for off- and on-road machines.

The problems related to using an electric motor with high overloads are obviously a very high armature-reaction-caused saturation, high Joule losses at low speeds and difficulties to deliver torque in the field weakening to reach the top speed needed.

There also seems to be a need to increase the synchronous inductance further and change the ratio of the magnetizing inductance and the leakage inductance in direction where the leakage is dominating. This helps in maintaining the PM flux and makes them less vulnerable to strong field weakening. These challenges can be solved by a TCPMSM in which the leakage inductance, $L_{\mathrm{s}\sigma}$, may be even larger than the magnetizing inductance, L_{m}. If the leakage inductance is dominating, the armature reaction remains small and the magnetic circuit saturation is not as obvious as in integral slot winding PMSMs. In addition, field weakening becomes easy, as there is a need to only limitedly affect the air gap flux linkage of the machine. Therefore, among different motor types a tooth-coil PMSM may be preferred for traction applications with field weakening.

A suitable TCPMSM can fulfil the demands of typical electric vehicle traction but will still be in difficulties in case of the torque-speed demands set by a heavy off-road machine load cycles when the machine is operated both off- and on-road [18]. A TCPMSM offers several alternatives to tune the ratio of the air gap leakage inductance, L_δ, and the magnetizing inductance, L_{m}, to reach a favourable field weakening range. The air-gap leakage inductance L_δ, depending on the leakage factor σ_δ, can be small or even tens of times the magnetizing inductance (see Table I) depending on the TCPMSM construction. L_δ is defined as

$$L_\delta = \sigma_\delta L_{\mathrm{m}}. \tag{3}$$

In an integrated solution, a suitable TCPMSM with a planetary gear offers a natural choice to reach a compact traction drive system. It is possible to build a TCPMSM around a

TABLE 1. TCPMSM parameters for different slot and polepair combinations.

Q_s \ $2p$		4	6	8	10	12	14	16	18	20
6	q G_δ k_w LCM QF	0.5 0.46 0.866 12 0.071		0.25 4.8 0.866 12 0.036	0.2 26 0.5 30 0.089		0.142 53 0.5 42 0.001	0.125 22 0.866 48 0.001		0.1 36 0.866 54 0.001
9	q G_δ k_w LCM QF		0.5 0.46 0.866 18 0.104	0.375 1.2 0.945 72 0.132	0.3 2.4 0.945 90 0.066	0.25 4.8 0.866 36 0.01	0.214 0.46 0.617 126 0.225	0.188 71 0.328 144 0.001		0.15 112 0.328 90 0.001
12	q G_δ k_w LCM QF			0.5 0.46 0.866 24 0.14	0.4 0.96 0.933 60 0.145		0.286 2.9 0.933 84 0.048	0.25 4.8 0.866 48 0.033		0.2 26 0.5 60 0.001
15	q G_δ k_w LCM QF				0.5 0.46 0.866 30 0.175		0.357 1.4 0.951 210 0.318	0.313 2.1 0.951 240 0.212		0.25 26 0.5 60 0.005
18	q G_δ k_w LCM QF					0.5 0.46 0.866 36 0.21	**0.43** **0.83** **0.902** **126** **0.368**	0.375 1.2 0.945 144 0.265		0.3 2.4 0.945 180 0.142
21	q G_δ k_w LCM QF						0.5 0.46 0.866 42 0.246	0.438 0.8 0.89 336 1.02		0.35 1.5 0.953 180 0.291
24	q G_δ k_w LCM QF							0.5 0.46 0.866 48 0.282		0.35 1.5 0.953 210 0.145

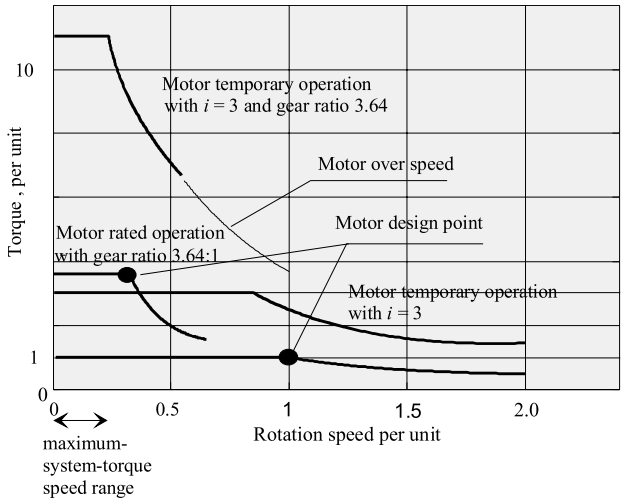

FIGURE 3. The operating areas, which can be fulfilled by using the motor with integrated two-step planetary gear switchable between gear ratios 3.64:1 and 1:1. The dots indicate the electrical machine design points with different gear ratios. The maximum-system output torque is $3.64 \times 3 = 11$ times the rated torque and 22 times the torque given at the maximum speed at constant power ($T_{\max\,\Omega} = 0.5$). If the gap between the high-current high-torque output (gear ratio 3.64:1) and the high-current output (gear-ratio 1:1) should be filled the motor should be driven deeper in the field weakening with high current and gear ratio 3.64:1. To reach the per-unit output speed 1 with gear needs the motor speed 3.64 per unit.

strong enough gearbox to achieve the shortest possible length and small enough diameter for the drive system. A TCPMSM is an obvious selection for this kind of integration because it can be easily realized as a thin rim around the gearbox and use the limited space in a wheel hub in an efficient way.

To reach a practical solution, a commercially available planetary gear with ratios of 3.64:1 and 1:1 is used in the proposed integrated drive system. If the TCPMSM per unit torque, $T_{\mathrm{e,pu}}$, is limited to 3 for lower speeds ($\omega_{\mathrm{s,pu}} < 0.5$) and if the TCPMSM can reach $\omega_{\mathrm{s,pu}} = 2$ per unit maximum speed and produce $T_{\mathrm{e,pu}} = 0.5$ in the constant power area, torque range will be 22:1 (11:0.5), which should be enough for many heavy off- and on-road machines. The target torque-speed curves of the integrated design with 1:1 and 3.64:1 gear ratios are illustrated in Fig.3. Here 1 p.u torque equals 324 Nm as a physical torque and 1. p.u speed equals 1200 min^{-1}, correspondingly.

The general layout of the system and a more detailed figure of the PMSM rotor and its integration with the sun gear are given in Fig. 4. The figure demonstrates how the different components can be arranged in the drive system. It is certain that a multiple-pole TCPMSM offers a large space for the gearbox inside the machine. To maximize the space inside the motor the rotor stack does not even have a separate frame inside it at all, but the stack itself works as a frame when pressed against a plate-like rotor body with long screws and an end plate. The basic idea behind the structure is that the screws and friction within the lamination together provide a core rigid enough to support itself. Tests on the rotor of the prototype motor have yielded good results.

It has to be stated, that the system inherently includes one extra feature as the planetary cogwheels need lubrication and the system will be partly filled with lubricating oil, which can also most efficiently be used as heat transfer medium in the machine. The rotor with embedded magnets is designed smooth to keep oil friction at a low level. The gear oil is pumped, filtered and cooled outside the motor. Linear magnetic actuators are used to operate the gear shifting.

III. DESIGN OF A TCPMSM WITH TWO-STEP PLANETARY GEAR BOX

In traction motor drives, the load cycle analysis forms the basis for the boundary conditions. In this case, such a work was performed in [19]. The motor design analysis is reported in details in [20], [21]. The viscous friction caused by the lubricating and cooling oil is minimized by smooth rotating surfaces and as large air gaps as possible. The smooth rotor surface and high air gap length however, are increasing the permanent magnet leakage but as important loss source in the design is the electric motor air gap friction it makes sense to invest a more in the permanent magnet material.

The selection of the slot/pole ($Q_s/(2p)$) combination for a TCPMSM plays a critical role in this study. Some important parameters for various slot/pole combinations are given in Table I. In the table, slots per pole and phase (q), air gap leakage factor (σ_δ), operating winding factor (k_w) and least common multiple (LCM) of the number of slots and poles are all provided.

The multi objective optimization based on particle swarm algorithm is used to investigate all suitable slot/pole combinations and to select the most suitable design. The optimization

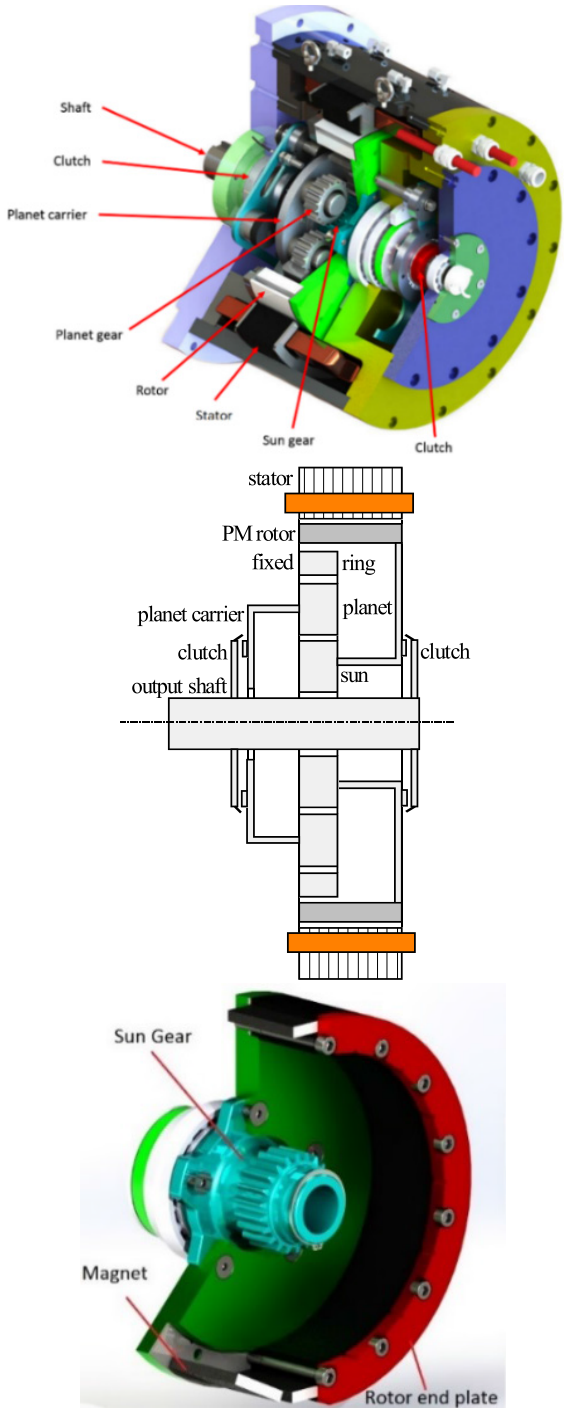

FIGURE 4. Overall view of the integrated hub motor, its schematics and a figure of the rotor alone. The TCPMSM rotor is fixed to the sun of the planetary gear.

problem has two input variables − the number of slots and the number of poles. The slot numbers vary from 6 to 72 and the pole number varies from 4 to 72. In the optimization, integer-slot and unbalanced winding configurations are sentenced and these configurations are eliminated. First of all, one needs to make the optimization criteria based on the application needs. From the problem introduction it is clear that a heavy duty off-road machine needs a lot of torque and

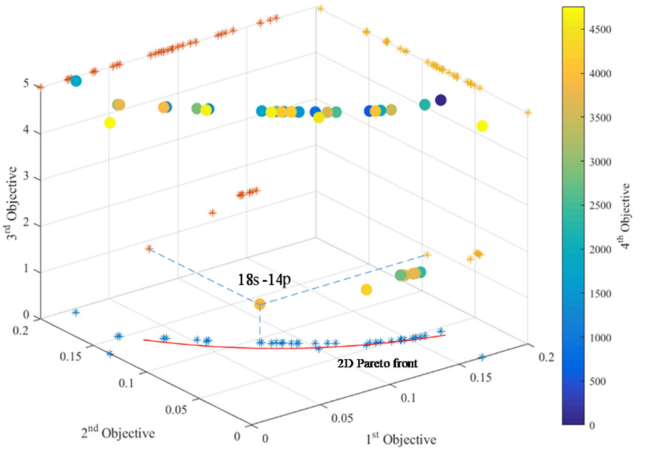

FIGURE 5. 4D visualization of the multi-objective optimization. The limit of the 3rd objective is set to 5 for better view.

speed is a subordinate demand. Also torque quality has a big importance. So, in optimization torque has a higher weight than speed. The optimization problem has four different cost functions defined as

$$f_1 = \text{Min}\,(\text{abs}\,(q - 0.5)) \tag{4}$$
$$f_2 = \text{Min}\,(\sigma_\delta) \tag{5}$$
$$f_3 = \text{Max}\,(k_\text{w}) \tag{6}$$
$$f_4 = \text{Min}\,(\text{abs}\,(\text{LCM} - 4830)) \tag{7}$$

The target of the 1st function is to approach $q = 0.5$ since the highest torque can be obtained at this value [25], and the 2nd cost function aims to minimize σ_δ and the 3rd function aims to maximize the k_w and the 4th function targets the maximum LCM that high LCM provides a good torque quality. The number of 4830 in (6) is the maximum LCM with these input variables. Minimizing σ_δ in this case is based on the fact that actually no large field-weakening area is needed in this very case. The maximum desired per-unit speed is 2.

The final result from the optimization point of view is the combination of all the different parameters. The results of the functions f_1-f_4 are multiplied with each other and one can get a quality factor QF listed in Table 1. The larger the QF is the better the machine fulfils the demands of the design target. Now all aspects, torque, torque quality and speed range are taken into account.

A 4-dimensional (4D) visualization of the multi-objective optimization is given in Fig. 5. The non-dominating results are illustrated with circles and 2D cut planes are illustrated with stars. It is easily seen in the 4D visualization that the 18-slot 14-pole is the most suitable slot/pole combination. This assumption can be also proven by 2D cut planes of the 1st vs the 2nd objectives. The 2D Pareto front can be easily seen in the figure and the closest result is obtained by the 18-slot 14-pole configuration. Fig. 6 shows the overall design flow of the proposed traction motor. The above-illustrated detail of the slot and pole selection is part of the flowchart. As Fig. 6 illustrates the integrated design starts with the dimensions of the planetary gear itself. The TCPMSM rotor

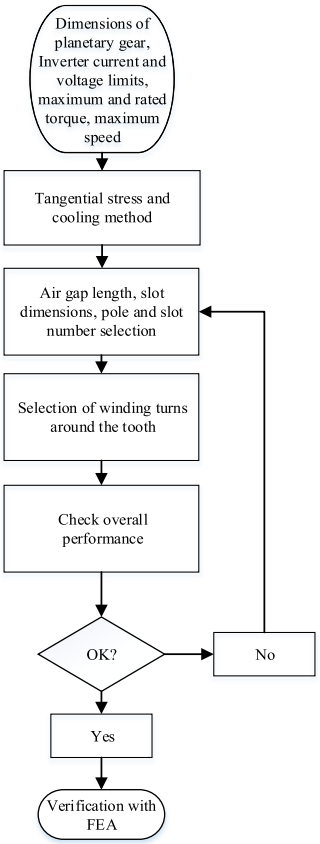

FIGURE 6. Flowchart of the integrated motor design process.

inner diameter D_{ri} must be larger than the planetary gear outer diameter. The gear properties and cogwheel speed limits dictate the maximum rotational speed of the motor. In this case, 1200 rpm was selected as the rated speed and 2400 rpm the maximum speed of the motor.

The grounds for selecting the 18/14 machine can be still summarized as: 1) It has been shown that tooth-coil machines with as high as possible number of slots per pole and phase have the best torque producing capability [25]. The value $q = 0.43$ is close to the limiting value of $q = 0.5$ beyond which we have distributed windings. The value of $q = 0.5$ offers high torque production but produces a poor torque quality with high torque ripple. 2) The air-gap leakage factor with $q = 0.43$ is moderate, $\sigma_\delta = 0.83$ resulting in a moderate stator leakage inductance which is now desirable as the field weakening range is not wide because the gearbox is to be used [22], [24]. 3) Also the operating harmonic ($v = 7$) winding factor is acceptably high, $k_w = 0.902$ resulting in low Joule losses. 4) The 18/14-machine configuration has a moderate LCM (126) resulting in almost purely sinusoidal back-electromotive force (EMF), and in torque smoothness. Based on these factors, the 18/14 machine is the best combination for the proposed integrated design as the result of the optimization analysis (highest QF) predicted. In [26] the authors have proposed the same selection but overall 18/14 machine has not been analyzed much in the literature.

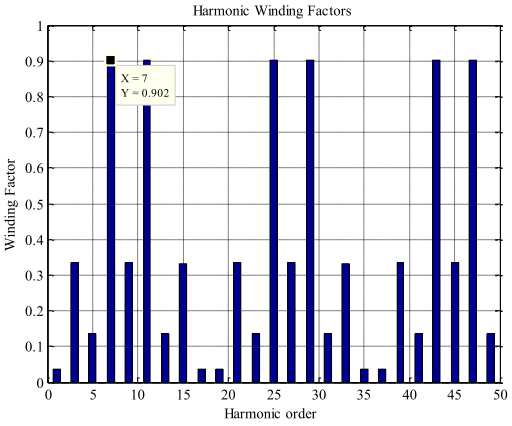

FIGURE 7. Harmonics created by the 18-slot winding in case of 14 poles. The machine operates with the 7th harmonic.

TABLE 2. Motor main characteristics.

Number of stator slots, Q_s	18
Number of rotor pole pairs, p	7
Number of slots per pole and phase, q	0.43
Length of the stator stack, l [mm]	75
Stator outer diameter, D_{se} [mm]	454
Stator inner diameter, D_s [mm]	346
Air gap, δ[mm]	3
Rotor yoke inner diameter, D_{ri} [mm]	280
Rotor yoke height [mm]	16.3
Slot average width [mm]	35
Stator yoke height [mm]	19.3
Number of coil turns in phase, N_{ph}	138
Phase resistance, R_s [p.u]	0.02
Induced voltage e_{PM} [p.u]	0.88
Rated and max frequency, f_N/ f_{max} [Hz]	140/280
Rated current, I_s [A]	67
Rated voltage, U_s [V]	400
Rated torque, T [Nm]	324

Figure 7 illustrates the winding factors of the different harmonics of the 18-slot 14-pole three-phase tooth-coil machine. The lowest strong harmonic – the seventh one – is used to operate the motor. A small fundamental winding factor $k_{w1} = 0.04$ also occurs. The low value of the fundamental is a benefit of this machine as it results in low rotor losses caused by the fast rotating armature fundamental.

The motor rated voltage and current are 400 V and 67 A. The rated-point current density in the stator copper is 4 A/mm^2. The rated tangential stress value of 24 kPa is but enables temporary overloading with 72 kPa. Table 2 presents the final design parameters.

Some details of the geometry of the TCPMSM are given in Fig. 8. Totally open slots are used to enable easy manufacturing of the winding. The coils can be manufactured outside of the machine and set on their places without deforming them. As mentioned above the rotor surface is smooth and the magnets are embedded in rotor laminations having a

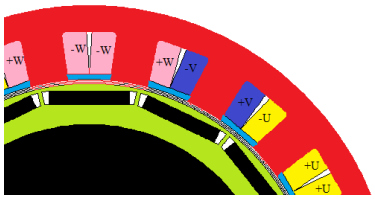

FIGURE 8. Magnetic circuit geometry. Smooth air gap guarantees a low friction. The flux barriers next to the magnets ensure low PM leakage.

thin yoke. The steel bridge over the magnets has a function of retaining the magnets but it also helps in collecting flux from the magnets to the open-slot teeth. Some increase in the q-axis armature reaction results from the permeance of the bridge. All these features, however, help in creating a machine for easy manufacturing and nice operating properties.

The proposed drive system employs direct oil cooling. In this oil-cooling concept, oil is circulated outside the motor for filtering and cooling. Cooled oil is pumped back to the motor through nozzles in the upper parts of the frame. The nozzles are placed so that the coils above the oil level will be flushed by the incoming cool oil. The cooling solution is presented in more details in [22].

The oil friction worst case value may be evaluated by the sentence assuming the whole air gap filled with oil

$$T_{\text{oil}} = \mu \frac{rS_{\text{r}}v}{\delta} = \mu \frac{rS_{\text{r}}2\pi r\Omega}{\delta} \tag{8}$$

where r is the radius measured from the rotor centre-line to the middle of the air gap, S_{r} is the rotor surface area facing the air gap, v is the linear speed of the rotor surface, Ω is the rotor angular velocity, δ is the air gap length and μ is the dynamic viscosity of hydraulic oil [22]. In the proposed drive system, air gap is only partly filled with oil and therefore an appropriate share of this value will be the practical result. The dimensioning of the planetary gear cogwheels dictates the desired viscosity level. In this case, the surface pressures of the cogwheels remain low, and therefore e.g. automatic transmission gear oil could be used inside the integrated design resulting in lower friction losses. Studies about the effectiveness of the oil cooling can be found e.g. in [22].

The mechanical strength of the rotor laminations was investigated at the nominal rotational speed by structural FEA and the stress contour is shown in Fig. 9. In the stress study, the radial force due to the magnets centrifugal force at the point is taken into account. Von Mises stress profile is obtained for the maximum torque value of 1000 Nm at the rated 1200 min^{-1} rotational speed. Similar evaluation was performed at the maximum speed. The magnetic steel yield strength value is in the range of 320 MPa, which is still acceptable for the material used.

The stress values stay in all cases on acceptable levels. Thus, it can be said that the mechanical strength of the rotor against centrifugal and torque forces is proven. As the rotor has no other frame than the laminated yoke, the tangential shear moving between the laminations is ensured by strong split pins and screws (Fig. 9). Fig. 9 also shows that the

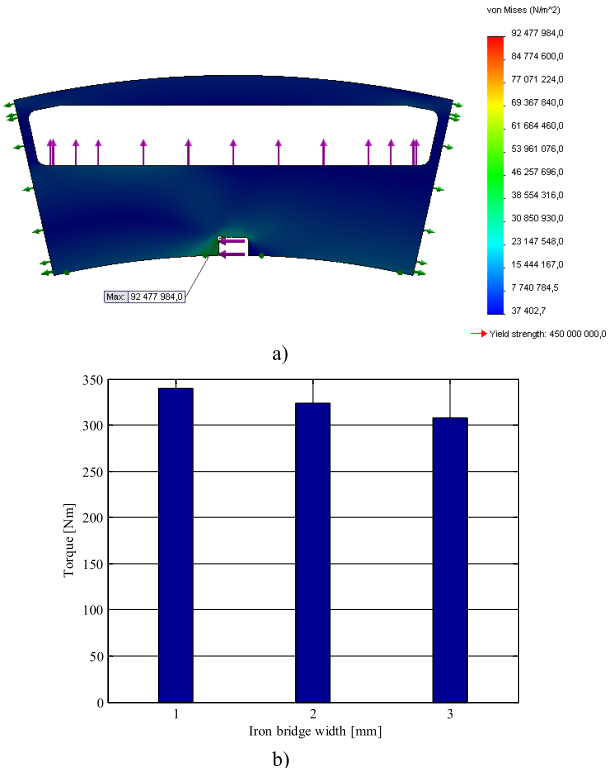

FIGURE 9. a) Von Mises stress levels in the rotor at maximum torque at rated speed 1200 min^{-1} b) electromagnetic torque-producing capability with the same q-axis current and different widths of iron bridges on the q-axes of the rotor.

thickness of the iron spokes retaining the rim has a significant effect on the torque production of the motor. Naturally, wide bridges enhance permanent magnet leakage flux but strengthen the rotor mechanically. Finally, 2 mm wide iron bridges were manufactured.

The planetary gear used in the prototype is a standard product of Sisu Axles [27]. It is originally used in Sisu's independent suspension axles GAWR and GCWR in high-speed on- and off-road applications as a wheel hub gear. The gear set has five planetary cogwheels and a drive ratio of 3.64:1, when the input is on sun gear and the output is on the planet carrier. The planetary gear is obviously over-dimensioned for the purpose of the prototype. Its manufacturer states that the gear can withstand torque inputs of up to 60 kNm before breaking. Some modifications have been made in the structure for the purposes of the prototype. Original planet cogwheels and their bearings have been employed, but the planet carrier has been redesigned to include a dog clutch for the gear ratio shifting. The teeth on the sun gear have the same dimensions as the original part, but the component now also has a flange for attaching it to the rotor, a machined surface for rotor bearings and a dog clutch for direct drive.

IV. MOTOR ELECTRO-MAGNETIC CALCULATION RESULTS

The motor geometry fine tuning was performed by using Altair Flux 2D FEA software to optimize the performance.

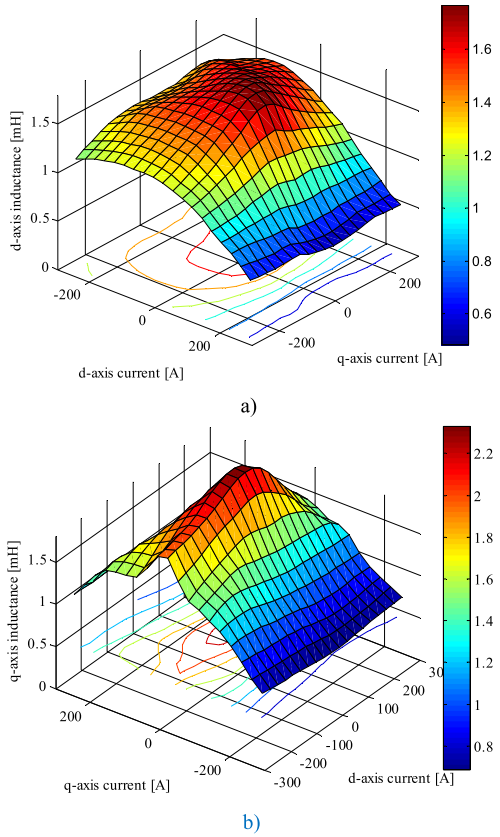

FIGURE 10. Synchronous incremental inductances of the proposed TCPMSM as a function of the of d- and q-axis currents a) d-axis incremental inductance b) q-axis incremental inductance. 1 mH corresponds to 0.26 per-unit inductance.

Flux linkages and synchronous inductances were obtained from static FEA when the coils were supplied by direct current and rotor was locked in q-axis or d-axis positions. Synchronous inductance increments for both axes are shown in Fig. 10. The incremental synchronous inductances can be determined numerically at locked rotor positions as follows

$$L_{\mathrm{d,inc}}\left(i_{\mathrm{d}}, i_{\mathrm{q}}\right) = \frac{\partial \psi_{\mathrm{d}}\left(i_{\mathrm{d}}, i_{\mathrm{q}}\right)}{\partial i_{\mathrm{d}}} \approx \frac{\Delta \psi_{\mathrm{d}}\left(i_{\mathrm{d}}, i_{\mathrm{q}}\right)}{\Delta i_{\mathrm{d}}}, \tag{9}$$

$$L_{\mathrm{q,inc}}\left(i_{\mathrm{d}}, i_{\mathrm{q}}\right) = \frac{\partial \psi_{\mathrm{q}}\left(i_{\mathrm{d}}, i_{\mathrm{q}}\right)}{\partial i_{\mathrm{q}}} \approx \frac{\Delta \psi_{\mathrm{q}}\left(i_{\mathrm{d}}, i_{\mathrm{q}}\right)}{\Delta i_{\mathrm{q}}}. \tag{10}$$

It is obvious that the synchronous inductances are strongly dependent on the axis currents. At no load, the TCPMSM is fairly non-salient, $L_{\mathrm{d}} \approx L_{\mathrm{q}}$. Saliency may be observed based on different saturations. Fairly strong cross-saturation phenomenon may also be observed. The d-axis incremental synchronous inductance stays moderately stable as a function of the q-axis current with $i_{\mathrm{d}} = 0$. The cross saturation drops $L_{\mathrm{d,inc}}$ from 1.5 mH at no load to about 1.2 mH at 200 A q-axis current with $i_{\mathrm{d}} = 0$.

The q-axis synchronous inductance has a strong self-saturation at low values of i_{q} which is natural as the magnet retaining ring starts to saturate under q-axis armature reaction. L_{q} is fairly insensitive to negative d-axis currents and therefore the cross-saturation does not affect the machine control significantly.

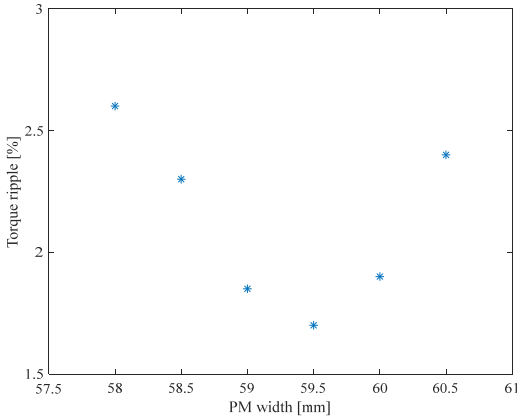

FIGURE 11. Motor torque ripple as a function of PM width at the rated operating point. Lowest torque ripple was found to be 1.7 %.

The torque output of the proposed TCPMSM with different PM widths was also investigated and the results are given in Fig. 11. The 324 Nm of average torque with 1.7% ripple is obtained and less than 0.1% of tooth harmonic cogging torque is observed. The results prove the design process in Section III.

V. PERFORMANCE AND LOSSES

Based on the analysis above, a 40 kW, 324 Nm, 18/14 TCPMSM prototype was built to verify the design analysis results. The power level of the machine was selected based on the power level of general working machine needs.

Fig. 12 presents the stator and rotor iron losses and permanent magnet eddy current losses calculated with FEA at different speeds. The stator Joule losses are dictated by the per-unit stator resistance indicating that at 40 kW output power the stator Joule loss will be about $P_{\mathrm{Cu}} = 1000$ W. The proportion of stator iron losses is not dramatically changing after the 1 p.u. speed as the field weakening starts there and the stator flux is reduced. Hence, also the stator iron losses are reduced.

A DC generator was used to load the motor. The oil level in the measurements was adjusted so that half of the standing motor was filled with oil. During operation, the oil flow rate was set to 3−5 l/min. Fig. 13 shows the test bench with measurement and additional equipment.

Measured induced voltage and 2 D and 3 D FEA calculated voltage curves from the cold machine (in temperature app. 20 °C) are shown in Fig. 14. The measured voltage correlates well with the calculated value (peak 295 V) and promises, therefore, a good performance. The amplitude of the induced voltage is slightly higher than the calculated one as the machine was cold at the moment of testing. The no-load voltage THD of the motor is less than 2 % consisting mostly of the 6^{th}, 12^{th}, and 18^{th} harmonics. This is a big benefit

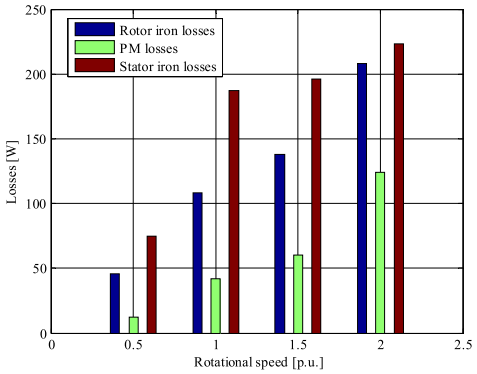

FIGURE 12. Speed dependent losses based on FEA.

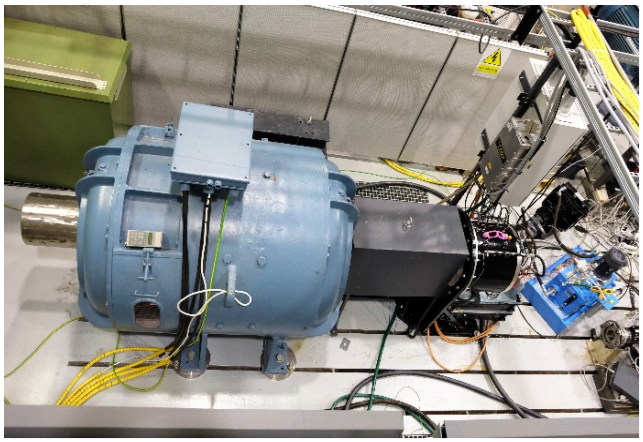

FIGURE 13. Test setup in laboratory. The large machine on the left is used to load the integrated PMSM (black machine on the right). Oil cooling laboratory system is seen on the right side of the figure.

of the 18/14 optimized construction. Stresses caused to the drive train are, in practice, free of torque ripple caused by the motor itself.

The efficiency map of the motor including the gear losses is shown in Fig. 16. It can be seen that the machine works efficiently and the efficiency-deteriorating effect of the planetary gear is small – in the range of 1–2 per-cent unit. Table 3 shows the values of iron losses and mechanical losses at the rated point of the machine. These losses have been measured from the no-load power. PM eddy current losses are negligible during no-load situation. The division between the iron losses and oil friction losses is assessed based on the FEA results for iron losses and assuming that all other losses from total losses are coming from oil friction. As it can be seen, the measured friction losses are considerably lower compared to what eq. (8) estimates.

The torque as a function of the rotational speed of the machine is given in Fig. 15. The figure focuses on the field weakening properties of the machine. At the same time, the figure shows that the required overload capability is achieved. All the curves in the figure are calculated results and some of the most important measurement points are marked with * to indicate the predicted performance of the prototype machine.

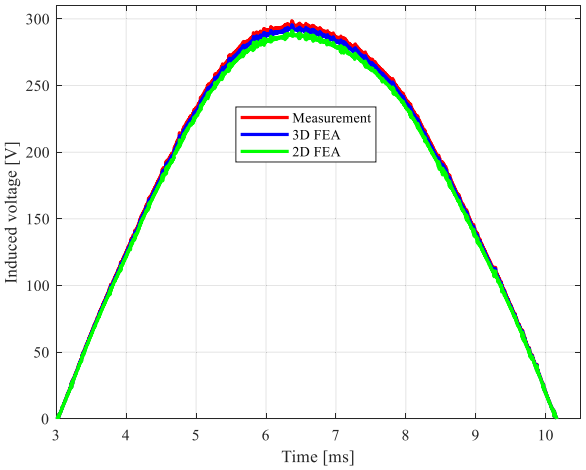

FIGURE 14. Measured no-load voltage waveform machine at 1 p.u. speed. It correlates well with the 2D and 3D FEA calculated no-noad voltages.

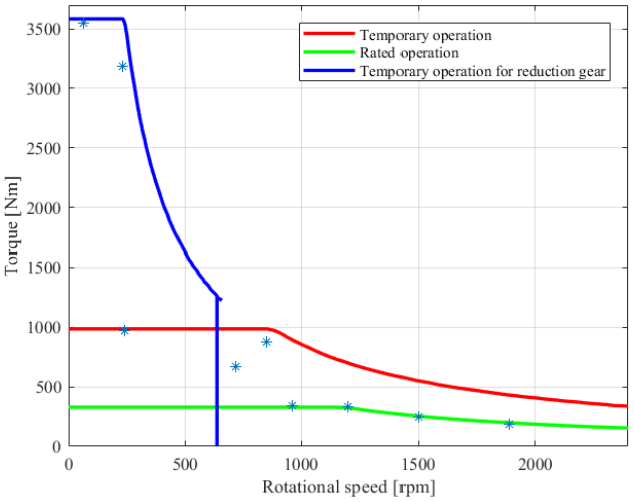

FIGURE 15. Torque curve as a function of rotational speed indicating the rated operation of the motor and temporary overload conditions for both gear ratios. The measured points are indicated by *. All the curves are the calculated ones.

TABLE 3. Machine losses at nominal speed.

Losses [W]	Calculated 2 D (rated)	Measured
Iron losses (incl.PM)	337	300
Oil friction losses	400	200
Stator Joule losses	1000	1000

Average temperatures of the windings as a function of rotational speed are measured and the temperature profile is given in Fig. 17. The results prove that the cooling method is efficient for the proposed drive system. Temperature values are averages from three phases at continuous state where the machine was heated for about half an hour. The tests show that the machine can be loaded continuously at about 50 kW power output. In traction motors the overload capability is the one of most important issues. The overload condition can be applied for 69 s and then the temperature limit 180 °C is reached, (Fig. 18.). The applied cooling method seems to be working efficiently.

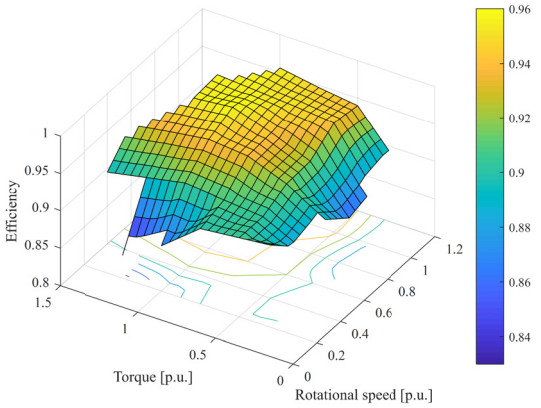

FIGURE 16. Measured efficiency map of the motor including the gear. The 1 per-unit speed and torque are the rated values of the motor. The peak efficiency of the motor corresponds well to the calculations made when assessing the hybrid drive train efficiency in Fig. 2.

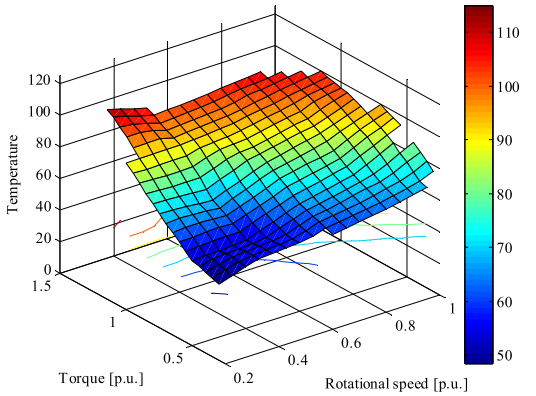

FIGURE 17. Average temperatures of the windings as a function of rotational speed and torque.

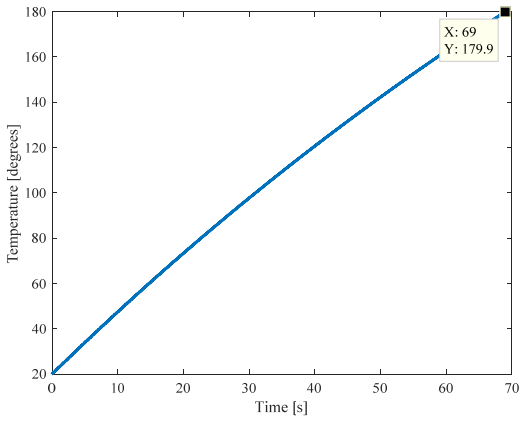

FIGURE 18. Temperature increase when the maximum torque at 3 p.u. current condition is applied. The machine can be used for c. 69 s with its maximum torque.

VI. CONCLUSION

A new integrated design was proposed for off- and on-road traction applications. The main practical purpose of the study was to find a good solution for a hub traction motor of e.g. an agricultural tractor, or a forest harvester. The proposed design consists of a tooth-coil permanent-magnet synchronous machine and a planetary gearbox. The selection of the TCPMSM parameters was investigated in details and a 4D multi-objective optimization was carried out to find the best suitable ($Q_s/(2p)$) combination of the proposed tooth-coil machine. The following aspects were considered to obtain the best traction motor parameters: 1) q close to 0.5, 2) high LCM, 3) high operating harmonic winding factor, k_w and 4) suitable air gap leakage factor, σ_δ. An 18-slot-14-pole TCPMSM was found as the optimum to be integrated with a planetary gearbox. The selection of the planetary gearbox and its implementation were explained in details and the proposed drive system was entirely explained. The on-load and no-load analyses of the proposed TCPMSM were investigated by FEA and the final design of the proposed motor was obtained by considering the planetary gearbox properties. A prototype was built and its experimental validation was performed. The results obtained from the design procedure of the proposed drive system and test are well matched even in extreme speed and torque limits.

REFERENCES

[1] J. Wu, J. Wang, C. Gan, Q. Sun, and W. Kong, "Efficiency optimization of PMSM drives using field-circuit coupled FEM for EV/HEV applications," *IEEE Access*, vol. 6, pp. 15192–15201, 2018.

[2] H.-C. Jung, G.-J. Park, D.-J. Kim, and S.-Y. Jung, "Optimal design and validation of IPMSM for maximum efficiency distribution compatible to energy consumption areas of HD-EV," *IEEE Trans. Magn.*, vol. 53, no. 6, Jun. 2017, Art. no. 8201904.

[3] J.-M. Mun, G.-J. Park, S.-H. Seo, D.-W. Kim, Y.-J. Kim, and S.-Y. Jung, "Design characteristics of IPMSM with wide constant power speed range for EV traction," *IEEE Trans. Magn.*, vol. 53, no. 6, Jun. 2017, Art. no. 8105104.

[4] M.-S. Lim, S.-H. Chai, and J.-P. Hong, "Design of saliency-based sensorless-controlled IPMSM with concentrated winding for EV traction," *IEEE Trans. Magn.*, vol. 52, no. 3, Mar. 2016, Art. no. 8200504.

[5] A. M. El-Refaie, "Fractional-slot concentrated-windings synchronous permanent magnet machines: Opportunities and challenges," *IEEE Trans. Ind. Electron.*, vol. 57, no. 1, pp. 107–121, Jan. 2010.

[6] L. Alberti, M. Barcaro, and N. Bianchi, "Design of a low-torque-ripple fractional-slot interior permanent-magnet motor," *IEEE Trans. Ind. Appl.*, vol. 50, no. 3, pp. 1801–1808, May/Jun. 2014.

[7] L. Yue, P. Yulong, Y. Yanjun, S. Yanwen, and C. Feng, "Increasing the saliency ratio of fractional slot concentrated winding interior permanent magnet synchronous motors," *IET Electr. Power Appl.*, vol. 9, no. 7, pp. 439–448, Jul. 2015.

[8] Z. Q. Zhu and Y. Liu, "Analysis of air-gap field modulation and magnetic gearing effect in fractional-slot concentrated-winding permanent-magnet synchronous machines," *IEEE Trans. Ind. Electron.*, vol. 65, no. 5, pp. 3688–3698, May 2018.

[9] S. Gerber and R.-J. Wang, "Cogging torque definitions for magnetic gears and magnetically geared electrical machines," *IEEE Trans. Magn.*, vol. 54, no. 4, Apr. 2018, Art. no. 8103209.

[10] X. Zhao and S. Niu, "Design and optimization of a new magnetic-geared pole-changing hybrid excitation machine," *IEEE Trans. Ind. Electron.*, vol. 64, no. 12, pp. 9943–9952, Dec. 2017.

[11] S. Pakdelian, M. Moosavi, H. A. Hussain, and H. A. Toliyat, "Control of an electric machine integrated with the trans-rotary magnetic gear in a motor drive train," *IEEE Trans. Ind. Appl.*, vol. 53, no. 1, pp. 106–114, Jan./Feb. 2017.

[12] C. Nutakor, J. Montonen, J. Nerg, J. Heikkinen, J. Sopanen, and J. Pyrhönen, "Development and validation of an integrated planetary gear set permanent magnet electric motor power loss model," *Tribology Int.*, vol. 124, pp. 34–45, Aug. 2018.

[13] P. Immonen, "Energy efficiency of a diesel-electric mobile working machine," Ph.D. dissertation, Acta Univ. Lappeenrantaensis, Lappeenranta, Finland, 2013.

[14] X. Liu, H. Chen, J. Zhao, and A. Belahcen, "Research on the performances and parameters of interior PMSM used for electric vehicles," *IEEE Trans. Ind. Electron.*, vol. 63, no. 6, pp. 3533–3545, Jun. 2016.
[15] J. de Santiago, H. Bernhoff, B. Ekergård, S. Eriksson, S. Ferhatovic, R. Waters, and M. Leijon, "Electrical motor drivelines in commercial all-electric vehicles: A review," *IEEE Trans. Veh. Technol.*, vol. 61, no. 2, pp. 475–484, Feb. 2012.
[16] J. Nerg, M. Rilla, V. Ruuskanen, J. Pyrhönen, and S. Ruotsalainen, "Design of direct-driven permanent magnet synchronous motors for an electric sports car," in *Proc. ICEM*, Marseille, France, Sep. 2012, pp. 177–182.
[17] J. Nerg, M. Rilla, V. Ruuskanen, J. Pyrhonen, and S. Ruotsalainen, "Direct-driven interior magnet permanent-magnet synchronous motors for a full electric sports car," *IEEE Trans. Ind. Electron.*, vol. 61, no. 8, pp. 4286–4294, Aug. 2014.
[18] P. B. Reddy, K.-K. Huh, and A. M. El-Refaie, "Generalized approach of stator shifting in interior permanent-magnet machines equipped with fractional-slot concentrated windings," *IEEE Trans. Ind. Electron.*, vol. 61, no. 9, pp. 5035–5046, Sep. 2014.
[19] J. Montonen, P. Lindh, and J. Pyrhönen, "Design process of traction motor having tooth coil windings," in *Proc. ICEM*, Marseille, France, Sep. 2012, pp. 1264–1268.
[20] P. Lindh, J. Montonen, P. Immonen, J. Tapia, and J. Pyrhönen, "Design of a traction motor with tooth-coil windings and embedded magnets," *IEEE Trans. Ind. Electron.*, vol. 61, no. 8, pp. 4306–4314, Aug. 2014.
[21] J. Montonen, S. Sinkko, P. Lindh, and J. Pyrhönen, "Design of a traction motor with two-step gearbox for high-torque applications," in *Proc. ICEM*, Berlin, Germany, Sep. 2014, pp. 1069–1075.
[22] J. Montonen, J. Nerg, M. Polikarpova, and J. Pyrhönen, "Integration principles and thermal analysis of an oil-cooled and-lubricated permanent magnet motor planetary gearbox drive system," *IEEE Access*, vol. 7, pp. 69108–69118, 2019.
[23] P. Ponomarev, "Tooth-coil permanent magnet synchronous machine design for special applications," Ph.D. dissertation, Acta Univ. Lappeenrantaensis, Lappeenranta, Finland, 2013.
[24] P. Ponomarev, P. Lindh, and J. Pyrhönen, "Effect of slot-and-pole combination on the leakage inductance and the performance of tooth-coil permanent-magnet synchronous machines," *IEEE Trans. Ind. Electron.*, vol. 60, no. 10, pp. 4310–4317, Oct. 2013.
[25] P. Salminen, T. Jokinen, and J. Pyrhönen, "Pull-out torque of fractional-slot PM-motors with concentrated winding," *IEE Proc.-Electr. Power Appl.*, vol. 152, no. 6, pp. 1440–1444, Nov. 2005.
[26] R. Dutta, L. Chong, and M. F. Rahman, "Design and experimental verification of an 18-Slot/14-pole fractional-slot concentrated winding interior permanent magnet machine," *IEEE Trans. Energy Convers.*, vol. 28, no. 1, pp. 181–190, Mar. 2013.
[27] *Sisu Axles From*. [Online]. Available: http://www.sisuaxles.com/en/c/document_library/get_file?uuid=f39d984a-6dc7-4314-ba8c-94f0470e4640&groupId=11705

JUHO MONTONEN was born in Joutseno, Finland, in 1988. He received the B.Sc. and M.Sc. degrees from the Lappeenranta University of Technology (LUT), Finland, in 2011 and 2012, respectively, where he is currently pursuing the Ph.D. degree.

His research interests include electrical machines and drives. His research works focus on permanent magnet motors, with a special reference to different kinds of traction applications.

JANNE NERG (M'99–SM'12) received the M.Sc. degree in electrical engineering, and the Licentiate of Science (technology) and D.Sc. (technology) degrees from the Lappeenranta University of Technology (LUT), Lappeenranta, Finland, in 1996, 1998, and 2000, respectively, where he is currently an Associate Professor with the Department of Electrical Engineering.

His research interests include the fields of electrical machines and drives, especially electromagnetic and thermal modeling and the design of electromagnetic devices.

MEHMET GULEC (S'12) received the B.S. and M.S. degrees in mechatronics engineering from Kocaeli University, Kocaeli, Turkey, in 2010 and 2013, respectively, where he is currently pursuing the Ph.D. degree with the Department of Mechatronics Engineering. He is doing his thesis with the Department of Electrical Engiinering, Lappeenranta University of Technology. Moreover, he is having a research exchange. He is also a Research Assistant with the Department of Mechatronics Engineering, Kocaeli University. His research interests include modeling, simulation, and design of electromagnetic systems and mechatronics.

JUHA PYRHÖNEN was born in Kuusankoski, Finland, in 1957. He received the D.Sc. degree from the Lappeenranta University of Technology (LUT), Finland, in 1991. He became an Associate Professor of electrical engineering with LUT, in 1993, and a Professor of electrical machines and drives, in 1997. He is currently the Head of the Department of Electrical Engineering, LUT, where he is currently involved in research and development of electric motors and electric drives.

His current research interests include different synchronous machines and drives, induction motors and drives, and solid-rotor high-speed induction machines and drives.